www.czasopisma.pan.pl PAN POLSKA AKADEMIA NAUK www.journals.pan.pl

Arch. Metall. Mater., Vol. 61 (2016), No 4, p. 2013–2020

DOI: 10.1515/amm-2016-0325

A. CWUDZIŃSKI*,#, J. JOWSA*, P. PRZEGRAŁEK**

INTERACTION OF LIQUID STEEL WITH MOULD FLUX IN CONTINUOUS CASTING BLOOM MOULD - NUMERICAL SIMULATIONS AND INDUSTRIAL EXPERIENCES

The device under examination is a mould of a capacity of 0.5 Mg and with inner cross-section of 280×400 mm. The virtual model of the facility under investigation was made using Gambit, DesignModeler and Meshing programs. Computer simulation of the liquid steel flow and mould flux behaviour in turbulent motion conditions was done using the Ansys-Fluent® computer program. On the basis of earlier researches the volume of fluid (VOF) model was applied. Based on computer simulations carried out, steel flow and flux behaviour fields and curves of flux mould entrainment concentration were obtained. The results obtained from numerical simulation were compared with the data obtained during bloom casting under industrial conditions. Based on the obtained information on the interaction of steel with mould flux, the region was determined, in which conditions likely to favour the entrainment of slag portions into the forming bloom exist.

1. Introduction

During continuous casting, steel gradually solidifies to form a continuous casting bloom, billet or slab. Frequent problems occurring during the continuous bloom casting process include: the segregation of elements, porosity, the occurrence of oscillation marks on the external bloom surface, and internal cracks [1-4]. Therefore, the selection of the parameters of mould operation, soft reduction, the temperature of casting and cooling of steel in individual zones of the casting machine should guarantee the stable formation of the shell and the uniform solidification of steel in the direction of the vertical slab axis [5-9]. In the continuous steel casting process, in the mould operation region, the selection of mould flux is an important issue [10]. The fundamental role of mould flux is to provide the proper lubrication of the mould wall surface in contact with the forming steel shell and the control of the heat exchange process in the primary cooling zone. In addition, the mould flux should protect the steel surface against the contact with the atmospheric air and assimilate non-metallic inclusions. After being applied to the steel surface, the mould flux is subject to gradual heating. The flux ingredients become sintered and then melt, forming liquid slag. During the casting process, the chemical composition of the mould flux may undergo modification as a result of interaction with the steel and non-metallic inclusions, which will affect its physicochemical properties [11-12]. As continuous steel casting progresses, hydrodynamic patterns form in the working space of the mould, which influence the motion of steel in the upper mould part [13-19]. The intensive steel circulation may lead to the formation of vortices that draw slag portions into the bulk of the steel. On the other hand, exceeding the critical steel velocity at the interface between the two phases initiates the entrainment of slag drops and their transfer to the steel. Therefore, the knowledge of the behaviour of steel and its influence on the slag flux in the mould provides a basis for the optimization of the process of continuous steel casting in the primary cooling zone. This paper presents the results of numerical simulation of steel motion in the bloom mould. A numerical model was employed for the visualization of slag flux behaviour on the steel surface under non-standard casting conditions, i.e. with a small immersion of the submerged entry nozzle in the steel at a normal casting speed and high casting speed. The results obtained from numerical simulation were compared with the data obtained during bloom casting under industrial conditions. Based on the obtained information on the interaction of steel with mould flux, the region was determined, in which conditions likely to favour the entrainment of slag portions into the forming bloom exist.

2. Characterization of the test facility and computing methodology

The device under examination is a mould of a capacity of 0.5 Mg and with inner cross-section of 280×400 mm. The mould being currently operated in industry is showed on figure 1a. A detailed description of the dimensions of the mould and position of submerged entry nozzle (SEN) is provided on figure 1b. The inner diameter of the submerged entry nozzle is 0.045 m. The virtual model of the facility under investigation was made using Gambit, DesignModeler and Meshing programs. The virtual model is composed of 730 thousand

* CZĘSTOCHOWA UNIVERSITY OF TECHNOLOGY, DEPARTMENT OF METALS EXTRACTION AND RECIRCULATION, FACULTY OF PRODUCTION ENGINEERING AND MATERIALS TECHNOLOGY, 19 ARMII KRAJOWEJ AVE, 42-200 CZESTOCHOWA, POLAND

** ARCELORMITTAL POLAND S.A., UNIT IN DĄBROWA GÓRNICZA, 92 J. PIŁSUDSKIEGO AV., 41-308 DĄBROWA GÓRNICZA, POLAND

Corresponding author: cwudzinski@wip.pcz.pl

hexahedron elements with a specially densified computational grid in the mould flux location zone. Computer simulation of the liquid steel flow and mould flux behaviour in turbulent motion conditions was done using the Ansys-Fluent® computer program. On the basis of earlier researches the volume of fluid (VOF) model was applied [20]. The VOF model relies that all fluids in the domain are not interpenetrating. For each phase the volume fraction of the phase in the computational cell is considered. In each control cell, the volume fraction of the phases sum to unity. In relation to volume fraction (α) in the cell for all fluids three conditions are possible:

$$\alpha = 0$$
$$\alpha = 1$$
$$0 < \alpha < 1$$

The momentum equation describing the phenomena under examination in the domain are as follows:

$$\frac{\partial}{\partial t}(\rho u) + \nabla(\rho u\ ) = \nabla\ p + \nabla(\tau) + \rho g + F_S \qquad (1)$$

where: t - stress tensor (Pa), r - density (kg/m^3), u - velocity (m/s), t - time (s), g - gravitational acceleration (m/s^2), F_s - surface tension force (N/m).

The momentum equation is dependent on the volume fractions of all phases through the properties of density and viscosity. Therefore for all phases, the averaged volume fractions of density and viscosity take on the following form:

$$\rho = \sum \alpha_p \rho_p \qquad (2)$$

$$\mu = \sum \alpha_p \mu_p \qquad (3)$$

where: μ - average viscosity (kg/m×s), μ_p - phase viscosity (kg/m·s), ρ_p - phase density (kg/m^3).

For the description of the turbulence motion of each phases through the mould, the Realizable k-e turbulence model were adopted. The employed turbulence model was successfully used for the description of turbulent motion in the tundish [21]. Physical quantities of liquid steel (s), mould flux (f) and air (a) were as follows: ρ_s 7010 kg/m^3, μ_s 0.007 kg/m·s, ρ_f 2500, μ_f 0.08 kg/m·s, ρ_a 1.225 kg/m^3, μ_a 0.000017 kg/m·s,$\sigma_{steel\text{-}flux}$ 1.5 N/m, $s_{steel\text{-}air}$ 1.6 N/m and $\sigma_{flux\text{-}air}$ 0.4 N/m [22-23]. At the inlet mould (end of SEN), liquid steel inflow of 6.39 kg/s was assumed. The initial liquid steel massflow corresponded to the sequence of continuous casting of 0.28×0.4 m concast blooms at a speed of 0.5 m/min. The system of equations forming the mathematical model of steel flow was solved by the method of control volumes by employing discretization of the second order upwind and presto using the sequential solver. The Pressure-Implicit with Splitting of Operators (PISO) algorithm was used for the description of the coupling of the pressure and velocity fields in the model being solved. For non-stationary computations the implicit scheme with a time step size of 0.01 s was used. Computer simulations were performed for non-standard continuous casting conditions, i.e. with a small immersion of the submerged entry nozzle in the steel and at an increased casting speed. In the first testing stage, the submerged entry nozzle was immersed in the steel at a depth of, respectively, 0.03, 0.02 and 0.01 m, in such a manner that the nozzle position was fixed, while the filling of mould with steel was subject to change. A 0.02 m-thick mould flux layer was uniformly distributed over the steel surface. In the first stage of testing, the steel was flowing into the mould at a mass flow rate of 6.39 kg/s. At the second testing stage, on the other hand, with a submerged entry nozzle immersion in the steel of 0.01 m and a slag layer thickness of 0.02 m, the steel mass flow rate was increased up to a value of 12.78 kg/s.

3. Numerical results and discussion

Based on computer simulations carried out, steel flow and flux behaviour fields and curves of flux mould entrainment concentration were obtained. Figure 2 shows steel flow fields in the plane situated in the central part of the examined facility, positioned in parallel to the longer side of the mould. It was noticed that, irrespective of the steel flow rate, an intensified steel circulation region formed at a level of about ¼ mould height, being the result of streams reversing in the direction of the free surface and descending towards the mould bottom – along the feeding stream. The backward stream is situated in the immediate vicinity of the narrower mould walls. The increase in steel mass flow rate of causes a deeper penetration of the feeding stream into the mould working space. The increase in flow rate did not cause any significant changes in the hydrodynamic pattern forming in the working space of the mould. In view of the fact that one of the main factors influencing the entrainment of the mould flux phase to the steel is the exceeding of the magnitude of the critical velocity at the interface between the both phases, the steel velocity values were determined in that region. Figure 3 shows steel velocity fields in the plane located 0.005 m from the initial mould flux level. In both cases, characteristic regions of increased steel velocity are visible, which are located near the mould corners. However, even in those regions, the magnitude of steel velocity does not exceed 0.02 m/s, which is a value almost 20 times smaller than the mean value assumed as critical. However, in computer simulation variants, where the submerged entry nozzle immersion depth was 0.01 m, the entrainment of flux to the steel bulk was recorded. Figure 4 shows the results of the examination of mould flux behaviour at the interface of the both phases for the steel flow rates under consideration. In the case of the steel flow rate of 6.39 kg/s, the flux moves towards the submerged entry nozzle, then drains along the nozzle wall and, in interaction with the feeding stream, it starts moving into the bulk of steel. The increase in steel flow rate causes the recorded phenomenon intensifies, which involves the transfer of the flux into a greater depth in the mould. For the assessment of the flux penetration depth, four reference transverse planes were set, positioned in parallel to the mould bottom and located at a depth of 0.02, 0.04, 0.05 and 0.07 m, respectively, from the level of submerged entry nozzle immersion in the mould (0.1 m). The results for the amount of “dragged” slag originated from the mould flux, given in mass fractions and referring to different submerged entry nozzle immersion depths, are shown in Figure 5. In the case of computer simulation for the steel flow rate of 6.39 kg/s, the mould flux attained a maximum penetration depth of 0.04 m. After approx. 15 seconds, duration

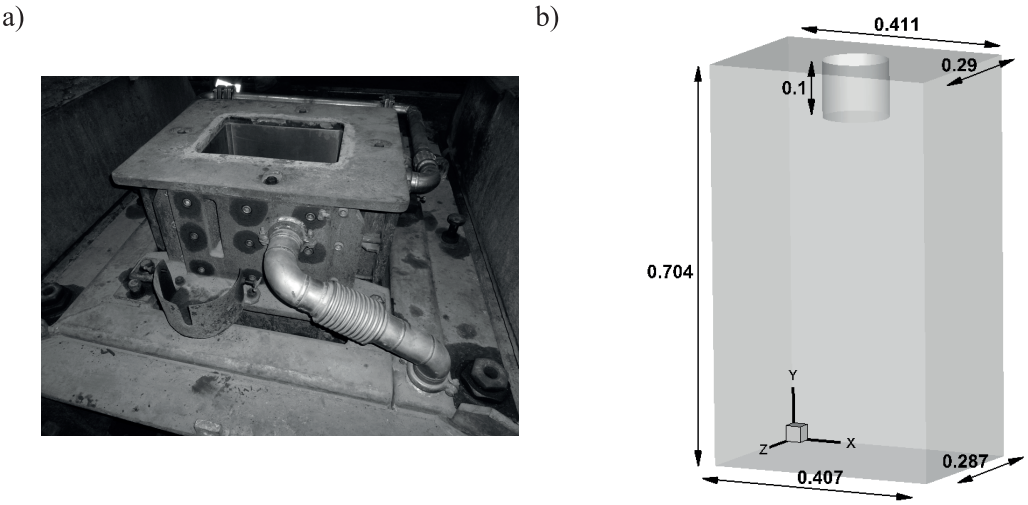

Fig. 1. Continuous casting bloom mould: a) industrial view, b) virtual model with position of SEN

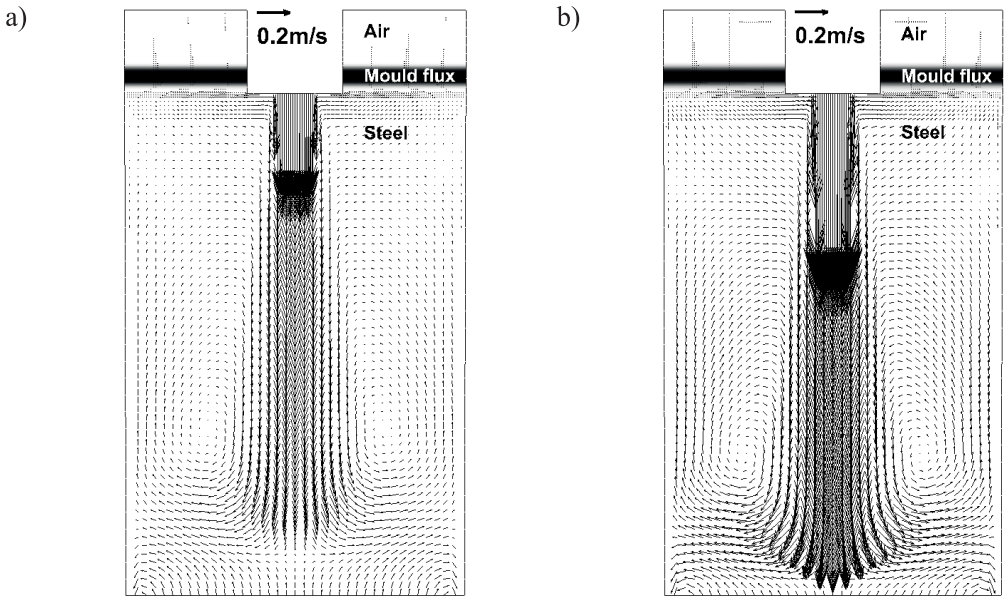

Fig.2. Hydrodynamic structure in the mould on the central plane: a) liquid steel inlet mass flow rate 6.39 kg/s, b) liquid steel inlet mass flow rate 12.78 kg/s

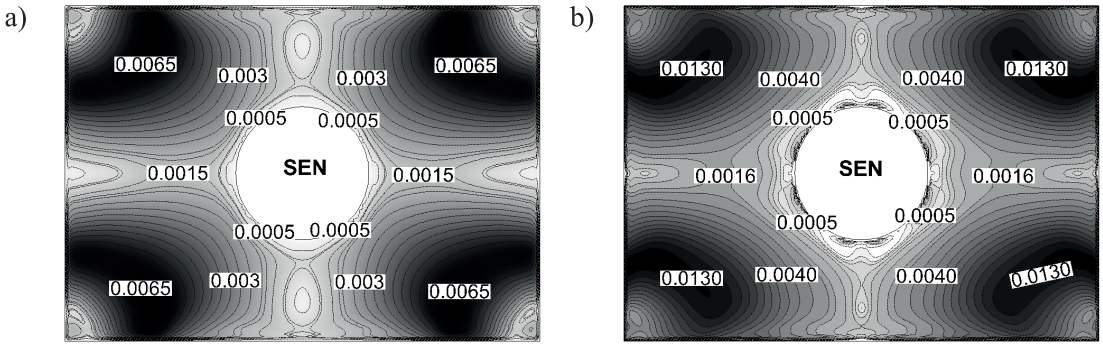

Fig.3. Liquid steel velocity field on the transversal plane localized 0.005 m below initial level of flux mould: a) liquid steel inlet mass flow rate 6.39 kg/s, b) liquid steel inlet mass flow rate 12.78 kg/s

of the slag phase "dragging" process decreased, reaching the submerged entry nozzle level and taking on the form of a slag "liquid icicle". By contrast, the increase of steel velocity in the feeding stream caused the mechanism of transferring the flux into the mould to intensify, and the flux was "dragged in" much deeper, which increased the "liquid icicle" size. However, even in the case of the steel flow rate increasing up to a level of 12.78 kg/s, no mould flux was recorded to occur at the mould bottom (outlet) level. From the computer simulations, the mould flux was not noticed to be carried over into the steel

in the form of drops, which precludes the Kelvin - Helmholtz instability mechanism, because the velocities of steel being in contact with the mould flux layer are not very high. To explain the occurred phenomenon of liquid slag draining along the SEN wall, the region, in which the phenomenon of mould flux transfer into the steel bulk might be initiated, was subjected to analysis. Figure 6 shows the motion of steel at the steel–mould flux interface. The initial region of mould flux position is denoted with black broken lines. Immediately at the submerged entry nozzle, a hydrodynamic pattern oriented from the steel–mould flux interface to the submerged entry nozzle forms, which is responsible for transferring the mould flux to the feeding stream-affected region. Therefore, after exceeding the critical depth, the hydrodynamic pattern occurred in the

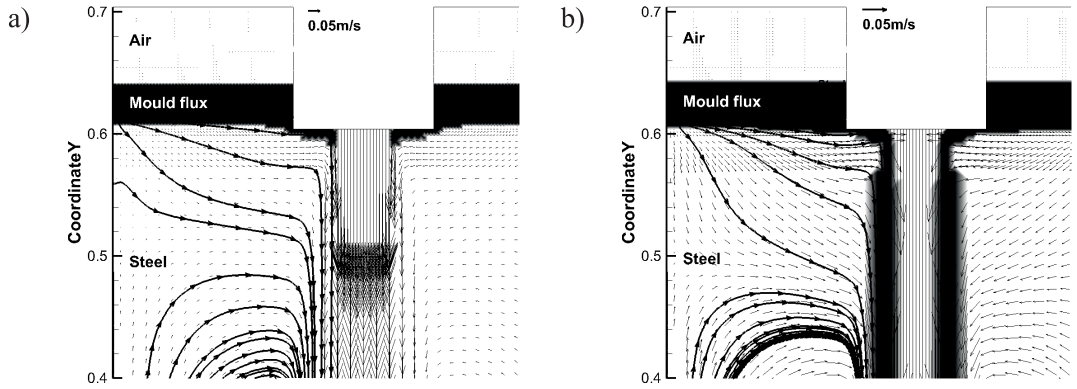

Fig.4. Behaviour of mould flux in the mould for case of SEN depth 0.01 m: a) liquid steel inlet mass flow rate 6.39 kg/s, b) liquid steel inlet mass flow rate 12.78 kg/s

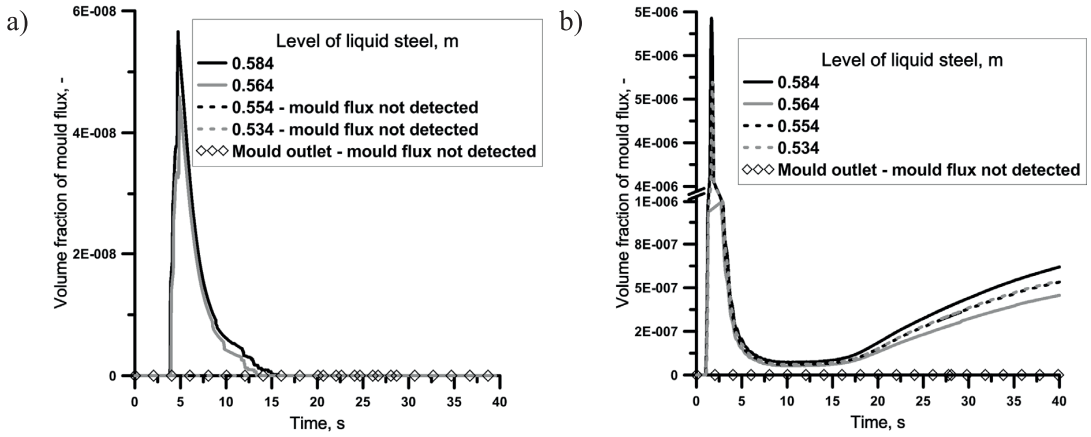

Fig.5. Average volume fraction of mould flux in liquid steel for case of SEN depth 0.01 m: a) liquid steel inlet mass flow rate 6.39 kg/s, b) liquid steel inlet mass flow rate 12.78 kg/s

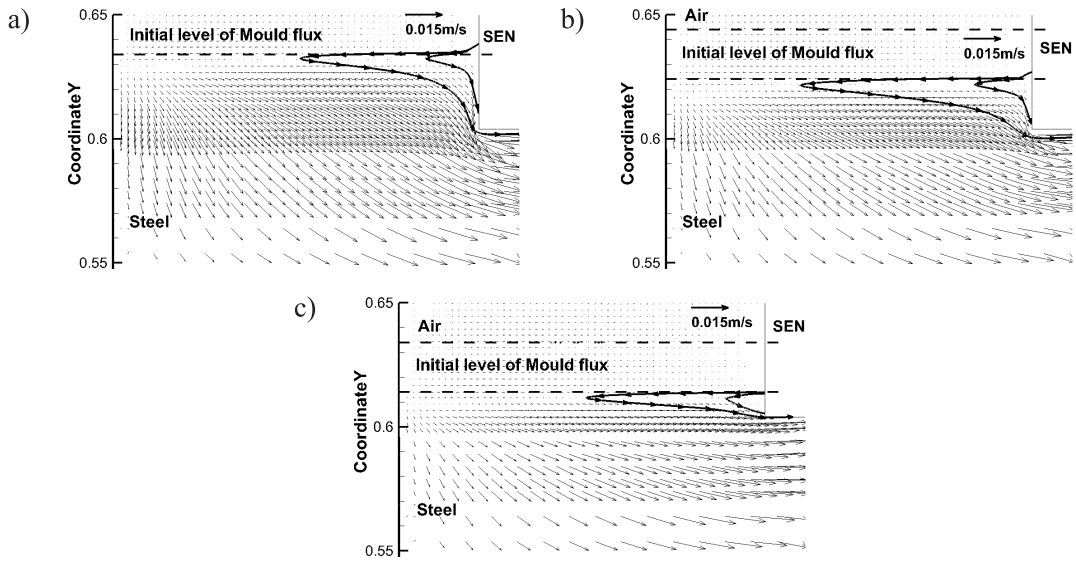

Fig.6. Direction of liquid steel flow near the initial level of flux mould: a) SEN depth 0.03 m, b) SEN depth 0.02 m, c) SEN depth 0.01 m

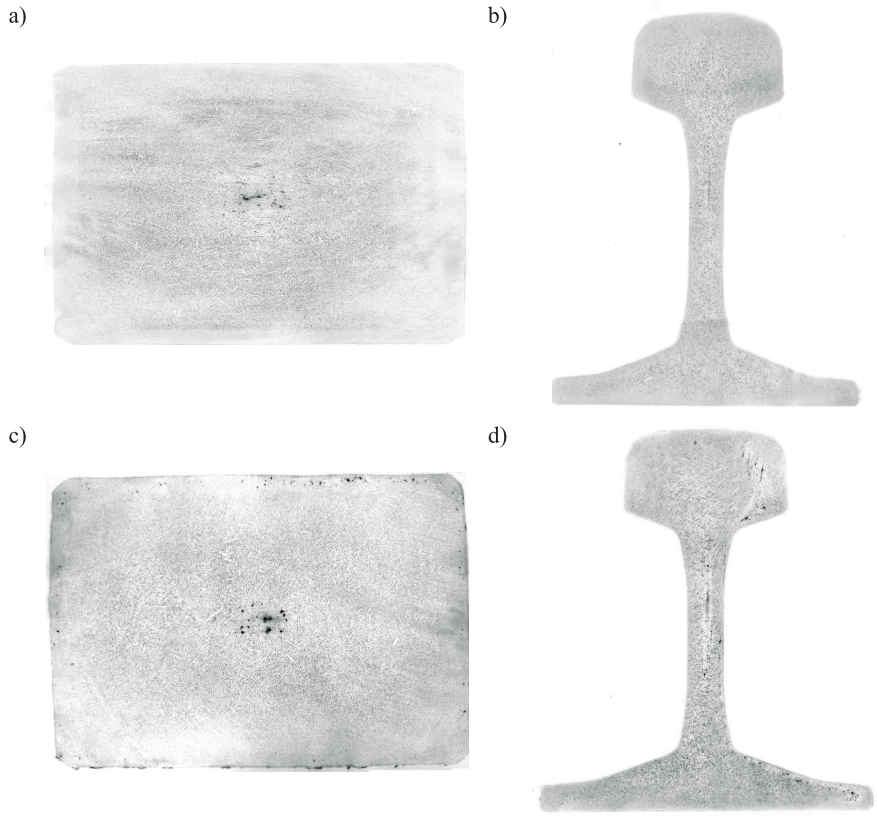

Fig.7. Baumann print: a) bloom with correct structure, b) final product with correct structure, c) bloom with mould flux marks, d) final product with mould flux marks

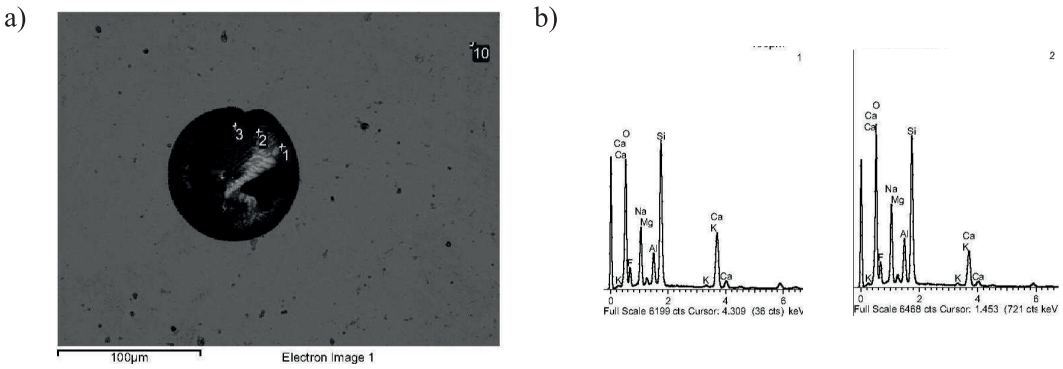

Fig.8. Characteristic non-metallic inclusion from bloom: a) microscopic view, b) chemical compositions

submerged entry nozzle region pushes the mould flux towards the nozzle, which, due to interaction with the feeding stream, is drawn under the nozzle. This suggests that a certain critical depth of submerged entry nozzle immersion in the steel exist, because, for the immersion depths of 0.03 and 0.02, not flux transfer under the submerged entry nozzle was noticed.

4. Industrial experiences

Blooms in the format of 280×400 mm are the feedstock for the long product rolling mill intended for rail production. Railway rail, as a responsible product, is checked with a flaw detector, which reveals any possible internal defects and enables the locations of their occurrence to be precisely determined. However, the examination with a flaw detector does not eliminate a scrap reject. Therefore, it is crucial to aim for reducing the quantity of internal rail defects detected on the flaw detector. One of the main causes of internal defects in rails are mould flux entrapments, as confirmed by the structural examination of blooms and rails. Figure 7 show an images of the correct internal structure of a bloom and a rail and structures of bloom and rail with defects. Both in the rail head and in the bloom, non-metallic inclusions appear, which are due to the entrapment of mould flux, which was confirmed by the chemical analysis of non-metallic inclusions, made using scanning electron microscopy. The analysis showed the occurrence of elements, such as Na, K and F, which are specific to mould flux (Fig.8). In view of the real problem, which is the entrainment of mould flux into the steel bloom, factors that might contribute to the above phenomenon were subjected to analysis. The factors covered by analysis were: tundish steel

temperature, casting speed, submerged entry nozzle immersion depth, and the type of mould flux. The exploration of industrial data allowed the correlation between the above-mentioned parameters and the rail defectiveness, as recorded on the flaw detector, to be determined. The defectiveness parameter meant the ratio of the quality of defective products to all products in the group under analysis. When examining the effect of the increase in tundish steel temperature, it was found that the increase in steel overheating relative to the casting temperature reduced the incidence of defects in final products. Warmer liquid steel more intensively transfers heat to the mould flux which, by warming up, more readily passes into the liquid state and gets lower viscosity, thus ensuring better conditions for mould wall lubrication and heat transfer. Obtaining a liquid, uniform structure of the flux leads to its gradual consumption during casting, thus reducing its residence time and accumulation on the mould liquid steel surface, which minimizes the risk of flux portions to be carried away by circulating liquid steel streams to the region, where bloom forms. The relationship between final product defectiveness and casting speed (Fig.9) and the depth of submerged entry nozzle immersion in the mould steel was also analyzed. The effect of casting speed was examined in the range of 0.45 - 0.6 m/min. In the examined casting speed range, the defectiveness of final products has acceptable level. A significant increase in rail defectiveness was found upon increasing the casting speed above a value of 0.6 m/min. The increase of casting speed has an immediate influence on the intensity of steel motion within the mould volume, also in the sub-meniscus zone, as this generates hydrodynamic patterns that might carry away mould flux portions into the bloom. No correlation was found between the final product defectiveness and the submerged entry nozzle immersion depth in the examined immersion depth range, that is from 0.03 to 0.07 m. During industrial trials, various mould flux types differing in their form (dusty or granular) and chemical composition were also tested. The form and chemical composition of the flux influence its melting point, viscosity and interfacial tension. The analysis of the final product defectiveness confirmed the relationship between the type of mould flux and the occurrence of defects originating from mould flux components. The results of the observations and examinations of the continuous steel casting process recorded under industrial conditions well correlated with the results obtained from computer simulations.

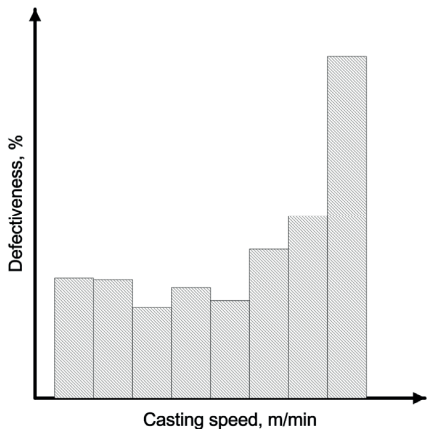

Fig. 9. Relationship between casting speed and defectiveness of final products

5. Summary

From the performed computer simulations and industrial trials it can be found that:

- In the 280×400 mm rectangular slab casting mould, steel circulation regions form, which are caused by the backward stream oriented towards the free steel surface;
- The process of transferring the mould flux directly towards the submerged entry nozzle walls and end is probably stimulated by the hydrodynamic patterns occurring in the immediate vicinity of the submerged entry nozzle;
- The initiation of the mould flux transfer under the submerged entry nozzle is dependent on the depth of submerged entry nozzle immersion;
- The increase in steel flow (casting speed) causes an increase in the depth of mould flux penetration into the steel volume;
- From the computer simulations, no entrainment of separate slag phase drops, being characteristic of the Kelvin - Helmholtz instability phenomenon, was found; hence, it can be inferred that the velocity of steel in the mould, in the immediate contact with the liquid slag, does not attain the critical values;
- At the next investigation stage, different mould flux types (their physicochemical properties) and casting speeds will be tested with the aim of determining the safe bloom casting speed for the quality of final products.

Acknowledgements

This scientific work has been financed from the resources of Ministry of Science and Higher Education as Statutory Researches

REFERENCES

[1] B. G. Thomas, M. S. Jenkins, R. B. Mahapatra, Ironmak. Steelmak. **31**, 485-494 (2004).
[2] O. Bode, K. Schwerdtfeger, H. G. Geck, F. Höfer, Ironmak. Steelmak. **35**, 137-145 (2008).
[3] Y. Chen, M. F. Xiao, G. R. Wu, J. Iron and Steel Res. **17**, 1-5 (2010).
[4] X. B. Li, H. Ding, Z. Y. Tang, J. C. He, Int. J. Miner. Met. Mater. **19**, 21-29 (2012).
[5] V. V. Kulakov, A. V. Yakovlev, T. N. Ryakhov, P. N. Tkachev, Y. E. Kan, Metallurgist. **30**, 398-399 (1986).
[6] T. Telejko, Z. Malinowski, M. Rywotycki, Arch. Met. Mater. **54**, 837-844 (2009).
[7] S. Luo, M. Y. Zhu, C. Ji, Y. Chen, Ironmak. Steelmak. **37**, 140-146 (2010).
[8] M. Alizadeh, Mat. Letters. **91**, 146-149 (2013).
[9] S. Ogibayashi, M. Kobayashi, M. Yamada, T. Mukai, ISIJ Int. **31**, 1400-1407 (1991).
[10] K. C. Mills, A. B. Fox, ISIJ Int. **43**, 1479-1486 (2003).
[11] A. Kiyose, K.-I. Miyazawa, W. Yamada, K. Watanabe, H. Takahashi, ISIJ Int. **36**, S155-S158 (1996).
[12] W. Wang, B. Lu, D. Xiao, Metall. Mater. Trans. B. **47**, 384-389 (2016).

[13] E. Torres-Alonso, R. D. Morales, S. García-Hernández, A. Najera-Bastida, A. Sandoval-Ramos, Metall. Mater. Trans. B. **39**, 840-852 (2008).
[14] Y. J. Xia, F. M. Wang, J. L. Wang, G. Z. Li, Int. J. Miner. Met. Mater. **18**, 562-569 (2011).
[15] H. Sun, J. Zhang, Metall. Mater. Trans. B. **45**, 1133-1149 (2014).
[16] Z. Zhao, H. Ni, H. Zhang, G. Chen, W. Yi, J. Hong, Ironmak. Steelmak. **41**, 539-546 (2014).
[17] Y. Tang, G. Hackl, G. Nitzl, C. Eglsäer, Proc. of 8th European Continuous Casting Conf., Graz, Austria, 487-497 (2014).
[18] M. Jeong, C. Choi, M. Y. Ha, S. J. Kim, J. K. Park, K. S. Oh, Met. Mater. Int. **21**, 303-310, (2015).
[19] H. Odenthal, I. Lemanowicz, R. Gorissen, H. Pfeifer, Metall. Mater. Trans. B. **33**, 163-172 (2002).
[20] E. Torres-Alonso, R. D. Morales, S. García-Hernández, J. Palafox-Ramos, Metall. Mater. Trans. B. **41**, 583-597 (2010).
[21] A. Cwudziński, Metall. Res. Tech. **111**, 45-55 (2014).
[22] S. Seetharaman (Ed.), A. McLean (Co-Ed.), R. Guthrie (Co-Ed.), S. Seetharaman (Co-Ed.), Treatise on Process Metallurgy, vol. 2, Process Phenomena, 2014, Elsevier.
[23] S. Seetharaman (Ed.), A. McLean (Co-Ed.), R. Guthrie (Co-Ed.), S. Seetharaman (Co-Ed.), Treatise on Process Metallurgy, vol. 3, Industrial Processes, 2014, Elsevier.